Proc. Natl. Acad. Sci. USA
Vol. 88, pp. 7066–7070, August 1991
Neurobiology

Spatial frequency tuning of single units in macaque supragranular striate cortex

(visual cortex/cortical maps/functional organization/cytochrome oxidase blob/interblob)

RICHARD T. BORN* AND ROGER B. H. TOOTELL

Department of Neurobiology, Harvard Medical School, 220 Longwood Avenue, Boston, MA 02115

Communicated by David H. Hubel, May 13, 1991

ABSTRACT **2-Deoxyglucose experiments have raised the possibility of a functional organization for spatial frequency in macaque striate cortex. To analyze this possibility with better spatial resolution, we made tangential microelectrode penetrations at constant eccentricity through supragranular striate cortex in 7 anesthetized, paralyzed macaque monkeys. We recorded from 121 single units. The data fell into two distinct populations with respect to mean preferred spatial frequency: (*i*) interblob cells (3.8 ± 2.0 cycles/degree, $n = 83$) and (*ii*) blob cells (1.1 ± 0.8 cycles/degree, $n = 38$; $P < 0.001$). Beyond this, we found no evidence for an orderly mapping of spatial frequency optima. At blob–interblob borders, we observed abrupt shifts from low, relatively uniform spatial frequency optima (blobs) to higher optima that varied unsystematically (interblobs). The spatial frequency optima (low vs. high) and nature of the tuning curves (low-pass vs. band-pass) in blob vs. interblob cells correlate well with psychophysical measures of the same differences for the chrominance vs. luminance channels. These data are consistent with a functional subdivision of striate cortex in which blob cells carry information concerned predominantly with color and interblob neurons carry information important for form analysis.**

Often, biologically relevant aspects of sensory stimuli are represented in a spatially orderly way across a two-dimensional sheet of neurons. This theme underlies the well-established concepts of cortical columns (1), functional architecture (2, 3), and cortical maps (4–6). In the visual system, maps of orientation selectivity and ocular dominance have been demonstrated in striate cortex of both the cat (2) and the macaque monkey (3) by electrophysiological techniques. Subsequently, these maps were confirmed using the functional neuroanatomical techniques of 2-deoxyglucose uptake (e.g., refs. 7 and 8) and optical recording (e.g., ref. 9).

A third variable, spatial frequency tuning, has been found to be represented nonhomogeneously in striate cortex (10–15). This suggests that a cortical map of spatial frequency exists. Such a conclusion would have significant consequences for the way we think about spatial vision, tending to favor models that make explicit use of local spatial frequency filters as basic building blocks of visual processing (16–22) over those that use feature detection (3, 23–26).

Since the pioneering work by Campbell and Robson (27) in psychophysics and Enroth-Cugell and Robson (28) on the physiology of retinal ganglion cells, a great deal of research has gone into the analysis of the spatial frequency filtering properties of neurons in the visual pathway. Neurons in striate cortex are reasonably selective for spatial frequency (29–33), and a distribution of tuning peaks is present within a small patch of cortex comparable in size to the hypercolumns described for orientation and ocular dominance (30, 33, 34). Furthermore, electrophysiological and 2-deoxyglucose studies of cat striate cortex appear to indicate the existence of cortical columns in which a given spatial frequency preference is constant (refs. 13 and 35, but see also refs. 10–12).

In macaques, 2-deoxyglucose experiments by Tootell *et al.* (14) have shown at least a coarse organization of striate cortex with respect to spatial frequency. Sinusoidal gratings of relatively high spatial frequency (5–7 cycles/degree) produced 2-deoxyglucose uptake confined to the interblob regions at 4–6 degrees of eccentricity, while low spatial frequency gratings (≈1 cycle/degree) produced uptake in the cytochrome oxidase blobs at the same eccentricity. The resolution of the 2-deoxyglucose technique is insufficient to allow one to decide between a continuous, unimodal distribution of spatial frequencies consistent with theories of an explicit mapping of spatial frequency (33) and a bimodal distribution of spatial frequency tuning corresponding to a functional division between blob and interblob pathways (14, 36, 37).

To help distinguish between these two possibilities, we recorded spatial frequency tuning curves of single units during tangential microelectrode penetrations through layers 2 and 3 of striate cortex of the anesthetized, paralyzed macaque monkey. We found that the distribution of spatial frequency tuning peaks was bimodal and did not vary continuously or smoothly as one would expect for a mapped variable (compare ref. 2).

In addition, we encountered a sizable proportion of interblob complex cells that could not be adequately characterized using spatially extended gratings because of side stopping. This property is interesting because of its high prevalence in supragranular striate cortex and its apparent absence at earlier stages. The nature of the inhibition and its anatomical localization will be addressed in the following paper (38). A preliminary account of this work has appeared (39).

MATERIALS AND METHODS

Experiments were performed on macaque monkeys (*Macaca fascicularis*) anesthetized with intravenous sufentanil (2–4 μg/kg of body weight per hr) and paralyzed with pancuronium bromide (0.15 mg/kg per hr). Adequacy of anesthesia was ensured by continuous monitoring of heart rate and electroencephalogram. Core body temperature and end-tidal P_{CO_2} were also monitored and maintained within physiological limits. The eyes were readied for the experiment as described (40).

A glass-coated tungsten microelectrode (modified from ref. 41) was advanced through a small craniotomy with a stepping motor microdrive. All penetrations were in striate cortex at an eccentricity of 5–6 degrees. During each penetration, several lesions were made by passing current (2 μA for 2–3 sec) through the recording electrode.

The publication costs of this article were defrayed in part by page charge payment. This article must therefore be hereby marked "*advertisement*" in accordance with 18 U.S.C. §1734 solely to indicate this fact.

*To whom reprint requests should be addressed.

At the end of an experiment the animal was deeply anesthetized with sodium pentobarbital (50 mg/kg) and perfused transcardially with fixative. The cortex was flattened (42), sectioned tangentially, and stained for cytochrome oxidase (43). Single units were categorized as being within blob or interblob regions (44, 45) by visual inspection of electrode track reconstructions superimposed on the cytochrome oxidase-stained tissue. For quantitative analyses, densitometric traces of these reconstructions were obtained using an image analyzer (Analytical Imaging Concepts, Roswell, GA). The optical density (3 × 3-pixel area) and distance from the center of the nearest blob were recorded for each unit's electrode track position, and, to allow comparisons between penetrations, the values were normalized.

Stimuli were generated by a Silicon Graphics IRIS 3130 computer and displayed on a Sony Trinitron color monitor with resolution of 1024 by 786 pixels at a 60-Hz noninterlaced refresh rate. The nonlinear relationship between the 8-bit digital gun values and phosphor luminance was corrected using look-up tables whose values were determined by calibration of the monitor with a Pritchard photometer. Single units were isolated on the basis of constant spike height and waveform. When a unit was encountered that could be clearly discriminated from the background activity, it was studied using a variety of stimuli including bars, spots, annuli, and gratings (square, sinusoidal, and rectangular wave) of chromatic and achromatic contrast. The optimal orientation, color combination, and ocular dominance class and the presence or absence of end-stopping were determined qualitatively by listening to the spike output on a loudspeaker. Interblob cells were classified as simple or complex according to the criteria of Hubel and Wiesel (2). Blob cells were classified according to the scheme of Livingstone and Hubel (36). After this, a spatial frequency tuning curve was determined by counting the total number of spikes in response to spatially extended sinusoidal gratings of various spatial frequencies at a constant temporal frequency of 2–3 cycles/sec. If the cell responded even moderately well to achromatic stimuli, then an achromatic grating was used to test spatial frequency tuning. Each stimulus was presented at least three times, for a period of 10 sec.

RESULTS

This study consisted of 17 tangential penetrations in seven animals. We recorded spatial frequency data from 121 single units: 38 (31%) units in cytochrome oxidase blobs and 83 (69%) in interblob regions. Of the 38 blob cells, 21 (55%) were strongly color-coded, giving little or no response to achromatic stimuli; these were tested with chromatic sinusoidal gratings (either red/green or blue/yellow). The remainder of the blob cells (17 of 38, 45%) and all interblob cells were tested with achromatic gratings. These relative proportions of different cell types were in good agreement with those obtained by others from layers 2 and 3 of parafoveal striate cortex (36). The interblob cells nearly always had complex receptive fields.

Fig. 1 shows examples of spatial frequency tuning curves for the different types of units we encountered (see *Insets*). The curves are typical of their respective receptive-field types and histologic locations (blob vs. interblob). The abscissas of these plots are identical to allow direct comparison of the spatial frequency optima and bandwidths of different units. The graphs illustrate the tendency for cells in the blobs to prefer low spatial frequencies and cells in the interblobs to prefer relatively higher spatial frequencies.

As shown in Fig. 2, most of the blob cells gave peak responses at spatial frequencies less than 2 cycles/degree (mean = 1.1, SD = 0.8), and most of them showed a rapid decrease in response at frequencies higher than optimum. Cells in the interblob regions, at the same eccentricity, had spatial frequency optima that were considerably higher (mean = 3.8 cycles/degree, $P < 0.001$) and more varied (SD = 2.0, $P < 0.05$). These cells usually showed a steep fall-off at the low frequency end of the spectrum, where the blob cells responded best.

To look for evidence of a systematic topographical mapping of peak spatial frequencies, we plotted the spatial frequency optimum of each cell as a function of its position along the electrode penetration (Figs. 3 and 4).

We found little evidence for a smooth and orderly progression of spatial frequency optima in any of the tangential penetrations through the upper layers of striate cortex. This is shown for a single penetration in Fig. 3, and for the entire

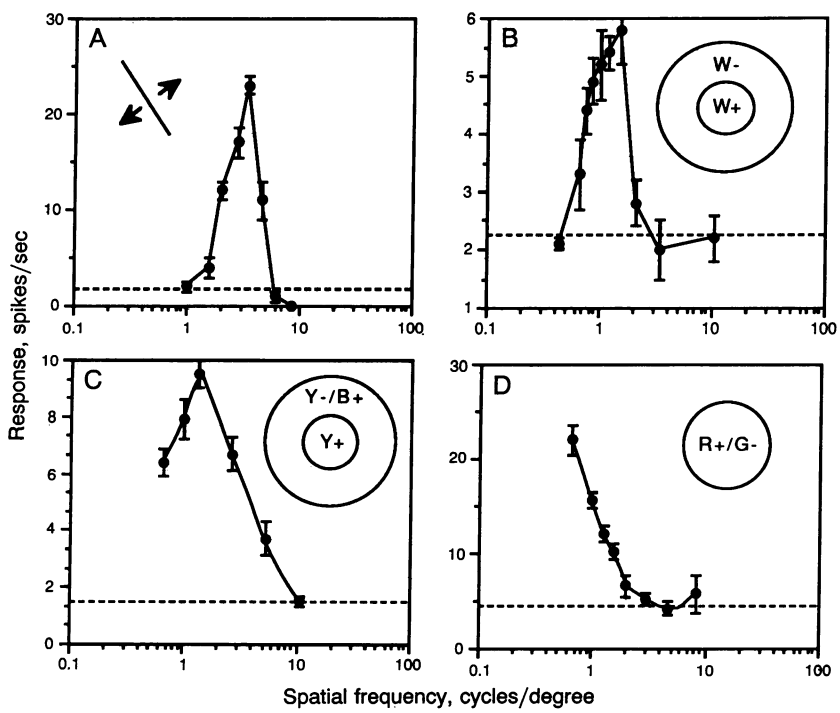

FIG. 1. Representative spatial frequency tuning curves for cell types encountered in layers 2 and 3 of macaque striate cortex. *Inset* in each graph shows the cell's receptive field as mapped with spots or bars of light [W, white (broad band); Y, yellow; B, blue; R, red; G, green]. *A* represents a complex cell from an interblob region. *B–D* represent blob cells: *B*, broad-band cell. *C*, yellow/blue 3/4 double-opponent; *D*, red/green, color-opponent center-only. The *x*-axes are all identical to permit direct comparison of spatial frequency optima. Note that for cells within blobs, the optima are typically around 1 cycle/degree, whereas the interblob cells generally prefer much higher spatial frequencies. Tuning curves for cells in *C* and *D* were determined using appropriate chromatically modulated sinusoidal gratings, since neither cell responded well to a pure luminance grating. Horizontal dotted lines represent the activity of the cell in response to a homogeneous field at the mean luminance of the gratings used to determine spatial frequency tuning.

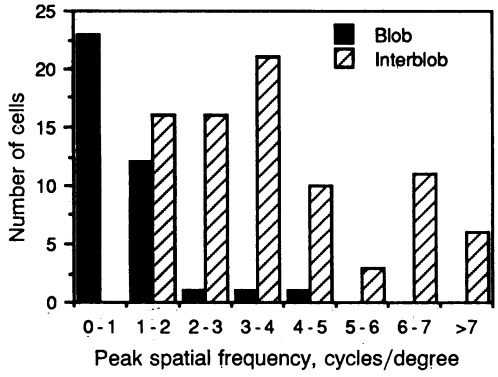

FIG. 2. Population histogram of spatial frequency optima for 121 unselected single units recorded from layers 2 and 3 of macaque striate cortex. Solid bars, cells located in cytochrome oxidase blobs (spatial frequency optimum, 1.1 ± 0.8 cycles/degree, mean ± SD, n = 38); hatched bars, cells located in interblob regions (spatial frequency optimum, 3.8 ± 2.0 cycles/degree, n = 83). The two populations were significantly different ($P < 0.001$) as determined by a two-sample t test for independent samples with unequal variances (Satterthwaite's method).

population of cells in Fig. 4. The results are the same whether one chooses optical density or distance from the nearest blob center as the independent variable.

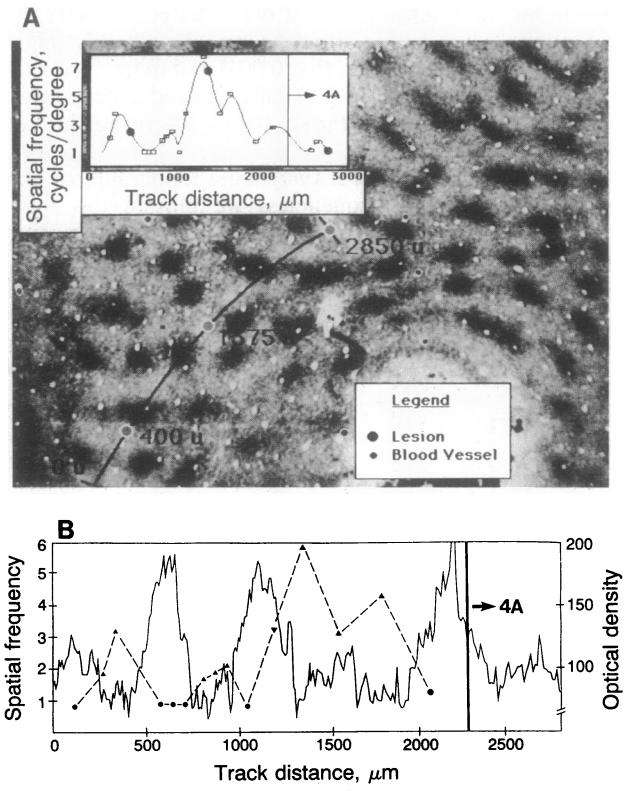

FIG. 3. Results from a tangential microelectrode penetration through layers 2 and 3 of striate cortex at an eccentricity of ≈5 degrees. (*A*) Electrode track reconstruction superimposed on a tangential section of striate cortex that has been stained for cytochrome oxidase (u, "microns"—i.e., μm). *Inset* is a plot of the spatial frequency tuning optima as a function of distance along the electrode track. The border between layers 3 and 4A is indicated by a solid vertical line. This graph is in vertical register with the histology below. (*B*) The same spatial-frequency-optimum data (dashed lines) superimposed on a densitometric scan (solid lines) of the cytochrome oxidase-stained tissue shown in *A*. Filled circles, non-orientation-selective units; filled triangles, orientation-selective units.

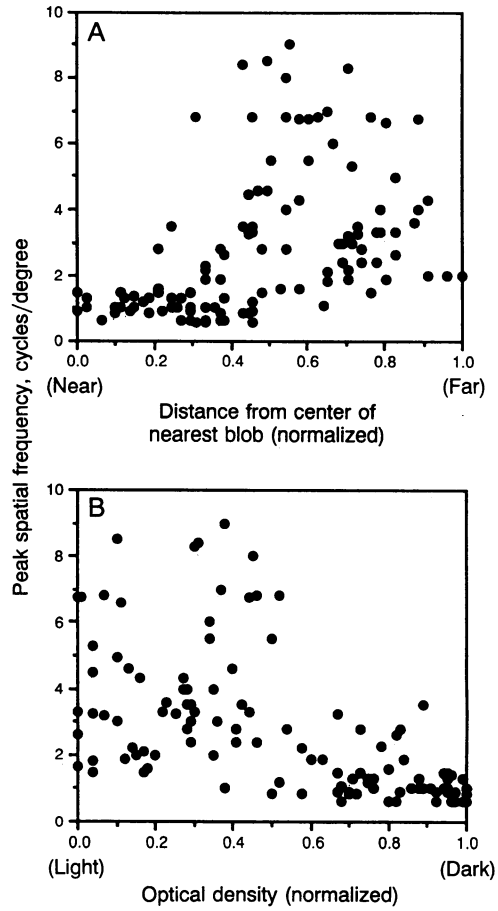

FIG. 4. Population summary of preferred spatial frequency vs. distance from the center of the nearest blob (*A*) and vs. optical density of cytochrome oxidase activity (*B*). Both graphs emphasize the tendency for blob cells to have low and uniform preferred spatial frequencies and for interblob cells to have higher and more varied preferred spatial frequencies. (*A*) These data were best fit by a step function: for distance < 0.40, preferred spatial frequency = 3.88 cycles/degree; for distance ≥ 0.40, preferred spatial frequency = 1.40. (*B*) These data were also best fit by a step function: for optical density ≤ 0.55, preferred spatial frequency = 4.12; for optical density > 0.55, preferred spatial frequency = 1.31.

The general result was that cells in blobs had low and relatively uniform preferred spatial frequencies, whereas interblob cells had higher preferred spatial frequencies that varied unsystematically from one location to the next. Blob–interblob transitions were as likely to show abrupt shifts in the preferred spatial frequency as they were to show intermediate values. This can be seen in the population data from Fig. 4 in which border cells (optical density of 0.4–0.6) show a wide scatter in their preferred spatial frequencies. It was also evident in some single penetrations, as shown in Fig. 5. During this penetration we observed a sudden shift from a preferred spatial frequency of 1 cycle/degree for a blob cell to 8 cycles/degree for the next recorded interblob cell only 50 μm further (Fig. 5, cells recorded at 500 and 550 μm). The change in preferred spatial frequency was accompanied by a change in the orientation selectivity: the blob cell was not orientation-selective whereas the interblob cell was sharply tuned for orientation. The occasional gaps of >50–100 μm were usually not due to a problem with sampling single units, but to the lack of response of the units in these interblob regions to extended gratings (starred arrowheads in Fig. 5).

The impressions one gets from visual inspection of the population data are borne out statistically. As noted above, the means and standard deviations of blob and interblob cells

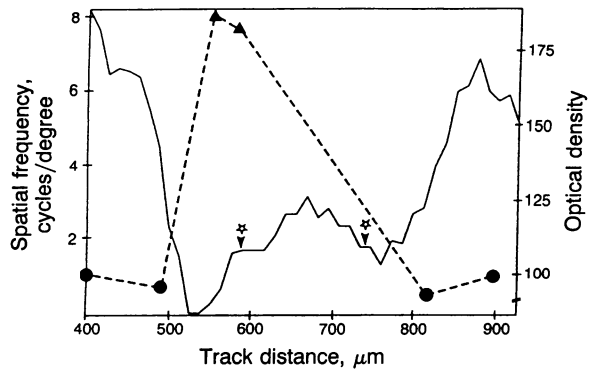

FIG. 5. Abrupt shifts in spatial frequency tuning of single units from the upper layers of striate cortex. The spatial frequency optima are plotted as a function of microelectrode track distance (dashed line) together with the optical density of the cytochrome oxidase-stained tissue (solid line). Filled circles, non-orientation-selective cells; filled triangles, orientation-selective cells. The two units at 590 and 740 μm (starred arrowheads) showed strong side inhibition, the second unit to such an extent that it would not respond to an extended grating of any spatial frequency.

are both significantly different. Simple linear regression shows a significant correlation between optical density (or distance from center of nearest blob) and preferred spatial frequency ($r^2 = 0.307$, $P < 0.01$, and $r^2 = 0.206$, $P < 0.01$, respectively); however, the data were fit better by a step function than by any of several continuous functions. The Marquardt–Levenberg algorithm was used to fit the data by the criterion of minimization of the square root of the residual sums of squares. For the plot of peak spatial frequency vs. optical density (Fig. 4*B*), this produced values of 19.23 for a linear model, 18.99 for a trigonometric model, and 17.67 for a step-function model. For the plot of peak spatial frequency vs. distance from the center of the nearest blob (Fig. 4*A*), the values were 20.59, 20.38, and 19.10, respectively. Furthermore, the improved fit with a step function was quite robust to changes in the exact location of the step: in the plot of preferred spatial frequency vs. optical density (Fig. 4*B*), step functions with the step at an optical density of 0.55, 0.60, or 0.65 all gave better fits than any of the continuous functions. Finally, if one confines one's attention to the interblob regions (e.g., optical density ≤0.60 in Fig. 4*B*), there is no tendency for preferred spatial frequency to correlate with optical density ($r^2 < 0.0001$, $P > 0.50$).

Further evidence against an orderly representation came from instances in which we recorded (*i*) two single units at one interblob electrode position that had very different spatial frequency tuning curves, (*ii*) very broad tuning curves for the multiunit activity, and (*iii*) single units and background activity that differed in preferred spatial frequencies.

DISCUSSION

Is There a Functional Organization for Spatial Frequency in Striate Cortex? We set out to look for a systematic mapping of spatial frequency optima for single neurons in layers 2 and 3 of striate cortex of the macaque monkey. Though we found the variations in spatial frequency tuning one would expect from earlier 2-deoxyglucose results (14), it was far from an orderly representation. The spatial frequency optima of cells within cytochrome oxidase blobs were low and relatively uniform, whereas those interblob cells that responded to extended sinusoidal gratings had higher spatial frequency preferences that tended to vary erratically from one location to the next. This contrasts markedly with the smooth progressions or orderly shifts one finds for orientation tuning and ocular dominance (46).

We also found that a high percentage of cells in the interblobs gave very poor responses to spatially extended gratings due to side inhibition. This made it difficult to establish a functional organization for spatial frequency, by precluding the measurement of a tuning curve in a considerable fraction of the cells. Furthermore, the prevalence of side inhibition raises questions as to the significance of the spatial frequency tuning curves that have been measured previously for upper-layer neurons. Some side-stopped cells *can* be induced to respond, at least grudgingly, to extended gratings of some spatial frequencies, particularly middle spatial frequencies. In such cells, however, the response to a single drifting bar or a delimited grating is invariably greater than the response to *any* extended grating. Thus, some "optimum" spatial frequency might be measured, but it is difficult to interpret, since the entire tuning curve is measured in the bottom fraction of the cell's dynamic range.

Our findings of a bimodal distribution of spatial frequencies and a lack of orderly progression of the optima conflict with the results of a previous study (15). Two main differences between the studies may explain this. First, the other study used recordings from multiple units at each location, whereas we measured responses from single units. We consistently found the interpretation of multiunit activity to be problematic for spatial frequency tuning. This is due to the scatter in spatial frequency tuning curves of cells in the interblobs as shown in the track reconstructions (see Fig. 3), recordings from two units at one location, and the broad spatial frequency tuning of the multiunit activity. The multiunit sampling used in the previous study would tend to smooth out the sudden shifts we observed at blob–interblob interfaces (Figs. 4 and 5) and could create an artifactual impression of progressive shifts in tuning.

The second source of discrepancy in the results arises from the use of only achromatic gratings in the prior analysis (15). For the strongly color-coded blob cells (55% of all blob cells in our sample), it was necessary to use chromatic gratings to obtain spatial frequency data, since these cells gave no response to black and white stimuli of any spatial pattern. They comprise a large part of our low-spatial-frequency (<2 cycles/degree) population of blob cells (see Fig. 2). This alone could explain the difference in population histograms obtained by the two groups.

Our evidence does suggest a functional dichotomy between the blobs and interblobs. As we will argue below, this supports the general notion of a subdivision of supragranular cortex into separate processing streams that has been proposed by others using different anatomical/physiological (36, 37, 47, 48) or theoretical (25, 49) criteria.

Blob Cells and Color Vision. We did not do quantitative tests to determine the precise chromatic properties of the cells we studied. We did, however, record from 21 single units, all within cytochrome oxidase blobs, that gave extremely poor responses to achromatic stimuli (whether spots, bars, annuli, or gratings) but gave strong responses to appropriately colored stimuli. We find it difficult not to think of these cells as conveying information about color. Furthermore, a number of previous reports have implicated blob cells in color processing (36, 50–52).

Many investigators have measured the sensitivity of human observers to equiluminant chromatic gratings as a function of the spatial frequency of the grating (53–60). Despite minor differences in methodology, the general consensus seems clear: for the detection of chromatically varying stimuli, the visual system behaves like a low-pass spatial frequency filter. This behavior contrasts with the band-pass spatial frequency behavior for detection of luminance-varying stimuli, at least at low temporal frequencies (60, 61).

Our measurements of the spatial frequency characteristics of blob vs. interblob cells in the macaque are consistent with

the above-mentioned properties of the human chrominance vs. luminance channels, respectively. We saw low-pass spatial frequency behavior (to spatially extended sinusoidal gratings) only in blob cells, and these same cells were strongly color-coded. Since the upper layers of area V1 are the predominant source of afferent projections to area V2 (62) and subsequent cortical visual areas, the spatial frequency tuning curves of blob cells provide further evidence for a role in color perception.

We thank David Hubel and Margaret Livingstone for thoughtful discussions and critical reviews of the manuscript. David Freeman and David Paul provided invaluable computer programming assistance, and Janet Robbins did some of the histology. This study was supported by the National Institute of Mental Health (MH14275-15) and the National Eye Institute (EY07980).

1. Mountcastle, V. B. (1957) *J. Neurophysiol.* **20,** 408–434.
2. Hubel, D. H. & Wiesel, T. N. (1962) *J. Physiol. (London)* **160,** 106–154.
3. Hubel, D. H. & Wiesel, T. N. (1977) *Proc. R. Soc. London Ser. B* **198,** 1–59.
4. Suga, N. (1982) in *Cortical Sensory Organization*, ed. Woolsey, C. N. (Humana, Clifton, NJ), Vol. 3, pp. 157–218.
5. Konishi, M. (1986) *Trends Neurosci.* **9,** 163–168.
6. Heiligenberg, W. (1987) *J. Comp. Physiol. A* **161,** 621–631.
7. Kennedy, C., Des Rosiers, M. H., Sakurada, O., Shinohara, M., Reivich, M., Jehle, H. W. & Sokoloff, L. (1976) *Proc. Natl. Acad. Sci. USA* **73,** 4230–4234.
8. Hubel, D. H., Wiesel, T. N. & Stryker, M. P. (1978) *J. Comp. Neurol.* **177,** 361–380.
9. Blasdel, G. G. & Salama, G. (1986) *Nature (London)* **321,** 579–585.
10. Maffei, L. & Fiorentini, A. (1977) *Vision Res.* **17,** 257–264.
11. Berardi, N., Bisti, S., Cattaneo, A., Fiorentini, A. & Maffei, L. (1982) *J. Physiol. (London)* **323,** 603–618.
12. Tolhurst, D. J. & Thompson, I. D. (1982) *Exp. Brain Res.* **48,** 217–227.
13. Tootell, R. B. H., Silverman, M. S., Switkes, E. & De Valois, R. L. (1981) *Science* **214,** 813–815.
14. Tootell, R. B. H., Silverman, M. S., Hamilton, S. L., Switkes, E. & De Valois, R. L. (1988) *J. Neurosci.* **8,** 1610–1624.
15. Silverman, M. S., Grosof, D. H., De Valois, R. L. & Elfar, S. D. (1989) *Proc. Natl. Acad. Sci. USA* **86,** 711–715.
16. Robson, J. G. (1975) in *Handbook of Perception*, eds. Carterette, E. C. & Friedman, M. P. (Academic, New York), Vol. 5, pp. 81–116.
17. Marcelja, S. (1980) *J. Opt. Soc. Am.* **70,** 1297–1300.
18. Daugman, J. C. (1980) *Vision Res.* **20,** 847–856.
19. Watson, A. B. (1983) in *Physical and Biological Processing of Images*, eds. Braddick, O. J. & Sleigh, A. C. (Springer, Berlin), pp. 100–114.
20. Wilson, H. R. & Gelb, D. J. (1984) *J. Opt. Soc. Am.* **73,** 1684–1690.
21. Klein, S. A. & Levi, D. M. (1985) *J. Opt. Soc. Am.* **A2,** 1170–1190.
22. Kulikowski, J. J. & Kranda, K. (1986) in *Visual Neuroscience*, eds. Pettigrew, J. D., Sanderson, K. J. & Levick, W. R. (Cambridge Univ. Press, Cambridge, U.K.), pp. 381–404.
23. Marr, D. (1982) *Vision* (Freeman, San Francisco).
24. Hildreth, E. C. (1985) *A. I. Memo No. 858* (MIT Artificial Intelligence Lab., Cambridge, MA), pp. 1–22.
25. Grossberg, S., Mingolla, E. & Todorovic, D. (1989) *IEEE Trans. Biomed. Eng.* **36,** 65–84.
26. Linsker, R. (1988) *Computer* **21,** 105–117.
27. Campbell, F. W. & Robson, J. G. (1968) *J. Physiol. (London)* **197,** 551–566.
28. Enroth-Cugell, C. & Robson, J. G. (1966) *J. Physiol. (London)* **187,** 517–552.
29. Maffei, L. & Fiorentini, A. (1973) *Vision Res.* **13,** 1255–1267.
30. Schiller, P. H., Finlay, B. L. & Volman, S. F. (1976) *J. Neurophysiol.* **39,** 1334–1351.
31. Albrecht, D. G. (1978) Doctoral dissertation (University of California, Berkeley, CA).
32. Movshon, J. A., Thompson, I. D. & Tolhurst, D. J. (1978) *J. Physiol. (London)* **283,** 101–120.
33. De Valois, R. L., Albrecht, D. G. & Thorell, L. G. (1982) *Vision Res.* **22,** 545–559.
34. Movshon, J. A., Thompson, I. D. & Tolhurst, D. J. (1978) *J. Physiol. (London)* **283,** 53–77.
35. Silverman, M. S. (1984) Doctoral dissertation (University of California, San Francisco, CA).
36. Livingstone, M. S. & Hubel, D. H. (1984) *J. Neurosci.* **4,** 309–356.
37. Blasdel, G. G. (1989) in *Sensory Processing in the Mammalian Brain*, ed. Lund, J. S. (Oxford Univ. Press, Oxford), pp. 242–267.
38. Born, R. T. & Tootell, R. B. H. (1991) *Proc. Natl. Acad. Sci. USA* **88,** 7071–7075.
39. Born, R. T. & Tootell, R. B. H. (1989) *Invest. Ophthalmol. Vis. Sci.* **30,** 111 (abstr.).
40. Tootell, R. B. H., Hamilton, S. L., Silverman, M. S. & Switkes, E. (1988) *J. Neurosci.* **8,** 1500–1530.
41. Merrill, E. G. & Ainsworth, A. (1972) *Med. Biol. Eng.* **10,** 662–672.
42. Tootell, R. B. H. & Silverman, M. S. (1985) *J. Neurosci. Methods* **15,** 177–190.
43. Wong-Riley, M. T. T. (1979) *Brain Res.* **171,** 11–28.
44. Horton, J. C. & Hubel, D. H. (1981) *Nature (London)* **292,** 762–764.
45. Hendrickson, A. E., Hunt, S. P. & Wu, J.-Y. (1981) *Nature (London)* **292,** 605–607.
46. Hubel, D. H. & Wiesel, T. N. (1968) *J. Physiol. (London)* **195,** 215–243.
47. Maunsell, J. H. R. & Newsome, W. T. (1987) *Annu. Rev. Neurosci.* **10,** 363–401.
48. DeYoe, E. A. & Van Essen, D. C. (1988) *Trends Neurosci.* **11,** 219–226.
49. Grossberg, S. & Mingolla, E. (1985) *Psychol. Rev.* **92,** 173–211.
50. Tootell, R. B. H., Silverman, M. S., Hamilton, S. L., Switkes, E. & De Valois, R. L. (1988) *J. Neurosci.* **8,** 1569–1593.
51. Ts'o, D. Y. & Gilbert, C. D. (1988) *J. Neurosci.* **8,** 1712–1727.
52. Lennie, P., Krauskopf, J. & Sclar, G. (1990) *J. Neurosci.* **10,** 649–669.
53. Schade, O. (1958) *J. SMPTE* **67,** 801–819.
54. Schober, H. & Munker, H. (1967) *Vision Res.* **7,** 1015–1026.
55. Green, D. G. (1968) *J. Physiol. (London)* **196,** 415–429.
56. Van Der Horst, G. J. C. & Bouman, M. A. (1969) *J. Opt. Soc. Am.* **59,** 1482–1488.
57. Granger, E. M. & Heurtley, J. C. (1973) *J. Opt. Soc. Am.* **63,** 1173–1174.
58. Kelly, D. H. (1983) *J. Opt. Soc. Am.* **73,** 742–750.
59. Noorlander, C., Koenderink, J. J., Den Ouden, R. J. & Edens, B. W. (1983) *Vision Res.* **23,** 1–11.
60. Mullen, K. T. (1985) *J. Physiol. (London)* **359,** 381–400.
61. Kelly, D. H. (1984) *J. Opt. Soc. Am.* **A1,** 107–113.
62. Kennedy, H. & Bullier, J. (1985) *J. Neurosci.* **5,** 2815–2830.